Astron. Astrophys. 173, 12–22 (1987)

ASTRONOMY AND ASTROPHYSICS

EVN and MERLIN observations of five superluminal radio sources

G. Pilbratt[1], **R. S. Booth**[1], **and R. W. Porcas**[2]

[1] Onsala Space Observatory, Chalmers University of Technology, S-43900 Onsala, Sweden
[2] Max-Planck-Institut für Radioastronomie, Auf dem Hügel 69, D-5300 Bonn 1, Federal Republic of Germany

Received July 24, accepted September 5, 1986

Summary. We report observations of five superluminal sources with the European VLBI Network (EVN) at 1.66 and 5 GHz, and MERLIN observations at 5 GHz. The observations were performed in an attempt to fill in the resolution gap between the milliarcsecond and arcsecond scales of previous observations; the sources observed were NRAO140, 3C120, 3C179, 3C279, and 3C345.

The hybrid maps constructed from these observations show that, save mainly for 3C120, neither the EVN nor the MERLIN maps show very much extended emission outside the respective cores. An analysis of the instrumental limitations shows that the lack of extended emission is not due to insufficient UV coverage. In fact, the quality of our maps is comparable to, or (in the case of MERLIN) better than that of the higher resolution maps showing the actual superluminal motion.

The conclusion is that on the angular scales of the present observations the intensity of the jet emission is lower than on smaller angular scales. On much larger angular scales local features of higher brightness occur. It appears that the mechanisms responsible for the observed more "blobby" radio emission on mas and arcsecond scales, whether extrinsic or intrinsic to the underlying "beam" itself, are not at work on these intermediate scales. We suggest that on the linear scales corresponding to the present observations the beams have generally more laminar flows, propagating with relatively small losses and thus having low radio brightness, especially compared to the core and emerging jet, and that the blobs of radio emission created near the core have faded. Our observations constrain any scheme requiring these jets to slow down from relativistic to subrelativistic velocities between the mas and arcsecond scales to do it without generating excessive amounts of radio emission.

Key words: active galaxies – jets of quasars – interferometry – VLBI – superluminal sources

1. Introduction

When variations in VLBI visibility curves on timescales of just a few months were first discovered more than a decade ago (Whitney et al., 1971; Cohen et al., 1971), the interpretation as rapid structural changes in quasar cores was not immediately accepted. Since then, a massive observing effort together with a dramatic improvement in data-reduction techniques, have produced indisputable observational evidence for structural changes in the form of systematic proper motion of one or several "knots" or "blobs" of radio emission away from an assumed stationary "core" (e.g. Pearson et al., 1981; Unwin et al., 1983, 1985; Walker et al., 1984; Walker, 1985). That the core really is stationary (with respect to another quasar) has now been demonstrated observationally in one case (3C345) by Bartel et al. (1984, 1986). When the observed angular motions of these blobs are converted into linear velocities (using a cosmological interpretation of the redshifts of the optical counterparts of the sources and a standard Friedmann cosmology), results range from a few to many times the speed of light. This phenomenon is now referred to as "superluminal motion". The blobs line up to form one-sided, often curved, jets on the milli-arcsecond (mas) scale. On angular scales of arcseconds jets still exist and are often curved in a manner suggestive of continuity with the mas scale jets (e.g. Browne et al., 1982).

The working hypothesis currently favoured to explain the measured superluminal motion involves relativistic bulk motion of the radiating plasma in a quasi-steady collimated beam, and a preferred geometry requiring the beam to point close to the line of sight towards the observer (Blandford and Königl. 1979). (In this paper the word "beam" will be used to denote the assumed underlying flow of physical material, whether radiating or not, while the word "jet" will refer to the actual appearance, on a radio map, of an elongated feature or a train of knots.) The nature of the moving blobs is unclear; they may be propagating shock waves caused either by instabilities within the beam (or the interface between the beam and surrounding medium) or by collisions between the flow and stationary condensations. The beams, however, are expected to be continuous from the core to the arcsecond and even larger angular scales where they supposedly power the extended radio lobes associated with large numbers of radio galaxies and quasars. In this model the observed jet curvatures may be the result of amplification of much smaller intrinsic curvatures by projection effects. Observational support for the existence of continuous beams comes from the detection of the jet in Cygnus A (Perley et al., 1984).

It is clearly of considerable interest to tie together the mas and arcsecond scale pictures, bridging the gap in resolution, and establishing an observational link between the pc-scale emission, showing proper motions, and that on the kpc-scale.

In this paper we report on an attempt to fill in the resolution gap for five superluminal sources. The observations have been carried out with the European VLBI Network (EVN) at two

Send offprint requests to: G. Pilbratt

Table 1. Dates for and antennas used in the observations

Source	Band[a]	Date	Antennas[b]	EVN point source calibrator(s)
NRAO140	*L*	13/14 Oct 1982	O J E D C	0235+164
	C	14/15 Dec 1982	O J_2 E W_{14}	0235+164
	C	20 May 1982	MERLIN[c]	–
3C120	*L*	12 Apr 1982	O J E D	BL Lac[d], OQ 208[d]
	C	8 Jun 1983	O J_2 E W_1 (T)[e]	DA 193
	C	11 Apr 1982	MERLIN[c]	–
3C179	*L*[f]	16 Apr 1982	O J E D	BL Lac[d]
	C	12/13 Dec 1982	O J_2 E W_{14}	DA 193
	C	15/16 Apr 1982	MERLIN[c]	–
3C279	*L*	27/28 Mar 1983	O J E W_{14} C T	None
	C	6 Jun 1983	O J_2 E W_7 (T)[e]	DA 193
	C	8/9 May 1982	MERLIN[c]	–
3C345	*L*	11 Oct 1982	O J E D C	BL Lac
	C	8/9 Jun 1983	O J_2 E W_1 (T)[e]	DA 193
	C	9/10 Apr 1982	MERLIN[c]	–

Notes

[a] EVN *L* band centre frequency 1661 MHz and *C* band centre frequency 4989 MHz, MERLIN centre frequency 4995 MHz

[b] For EVN antennas, see Table 2

[c] MERLIN consisted of the Jodrell Mk2, Knockin, Defford, Tabley, and Darnhall antennas in these observations

[d] No Jodrell data for the calibrator(s)

[e] Torun participated in the observations, but unfortunately no fringes were found

[f] 1613 MHz centre frequency

frequencies, 1.66 and 5 GHz (resolution ~10 or ~30 mas, and ~10 mas, respectively), and with MERLIN at 5 GHz (resolution ~80 mas). Our source sample consists of NRAO140, 3C120, 3C179, 3C279, and 3C345, i.e. all the known superluminals at the time when this project was initiated except 3C273, which is being studied separately.

2. Observations and data reduction

The EVN observations took place in five separate observing sessions during the period between April 1982 and June 1983. We obtained full tracks using arrays of four to six telescopes on all five sources at both frequencies. The actual observing dates and the telescopes used in each particular observation are given in Table 1, while relevant telescope characteristics are summarized in Table 2.

In all observations we used the MkII recording system with 1.8 MHz effective bandwidth (Clark, 1973). The cross-correlation was performed using the three-station MkII VLBI processor at the Max-Planck-Institut für Radioastronomie (MPIfR) in Bonn. For each observing session, the raw correlator output, consisting of sine and cosine correlations, was coherently averaged over typically one minute in order to increase the signal-to-noise ratio, taking coherence losses into account where appropriate. The averaged data sets were calibrated and edited. The calibration scheme used was that of Cohen et al. (1975) using the sensitivities, gain curves and measured system temperatures of the individual telescopes together with source fluxes measured simultaneously at Effelsberg. For the Effelsberg antenna, the actual measured antenna temperatures were used instead of calculated ones; at Westerbork an online calibration system compensates gain changes due to elevation, varying collecting area and other effects. After calibration the data was edited in the sense that obviously erroneous visibilities were flagged, and then neglected in the mapping process. The number of visibilities flagged was generally small, typically a few percent. However, in the case of 3C120 data from all baselines involving Jodrell Bank, and in the case of 3C279 data from all baselines involving Crimea, were somewhat more extensively edited in the 1.66 GHz observations. Finally, in order to obtain the best possible absolute flux values in the maps, comparisons with assumed unresolved calibrators were made where available (see Table 1), the fluxes of which were measured at Effelsberg during the observations, according to the scale of Baars et al. (1977). The corrections at this stage ranged up to 15% and they were applied to stations only (not to baselines) to safeguard against introducing non-closing errors (i.e. because in principle the calibrator could be resolved on some baselines, although there is nothing in the data to suggest that this is the case).

The MERLIN observations were conducted in April and May 1982, using an array of five antennas and a bandwidth of 10 MHz. For details see Table 1. Originally the MERLIN data were calibrated baseline by baseline in a manner very similar to that used for the EVN data, or with a rudimentary version of the much more sophisticated calibration software now in regular use. Recently, these data, with the exception of 3C179 and 3C279, have been recalibrated using the most up-to-date software which

Table 2. Basic data for the EVN antennas

Antenna and designation		Diameter (m)	Jy/K factor[a]		Typical T_{sys} (K)	
			L/*C* band		*L*/*C* band	
Onsala 25	O	26	10.8	17.0	25	45
Jodrell MkIA	J	76	1.24	–	65	–
Jodrell Mk2	J_2	25	–	13.2	–	120
Effelsberg	E	100	0.69	0.75	60	80
Dwingeloo	D	25	9.07	–	35	–
Westerbork[b]	W_n	n × 25	–	[b]	–	[b]
Crimea	C	22	18.4	–	120	–
Torun	T	15	[c]	–	[c]	–

Notes

[a] Typical value used, some stations supplied slightly different values on consecutive observing sessions

[b] Westerbork = Westerbork Synthesis Radio Telescope (WSRT), up to 14 25 m dishes. Online calibration software corrects for effects of shadowing, varying number (n) of dishes, elevation, system temperatures, etc.

[c] Torun had a system temperature of 4500/(Jy/K) K

not only calibrates amplitude and phase, but also attempts to correct for instrumental non-closing effects by deriving and applying baseline-dependent corrections to the data (Muxlow, 1986). The absolute flux calibration was derived from measurements of 3C84 (assumed 60 Jy) and checked using the source 3C287.

The calibrated and edited UV-data sets were mapped on the Onsala Modcomp Classic and Norsk Data ND570 computers, using the NRAO AIPS package, with the exception of the MERLIN 3C179 data which were mapped at Jodrell Bank shortly following the observations. An assessment of the fringe visibilities showed that the source structures were generally not very complicated and so for all maps a point source was used as input for the first iteration in the hybrid mapping process. Typically after three iterations, solving for the phases only in the self-calibration (selfcal) stage (e.g. Pearson and Readhead, 1984), the fit to the phases was very good, to the amplitudes very reasonable, and constant from one iteration to another. Up to this point the mapping procedure is relatively straightforward. The application of amplitude corrections to the telescope gains in selfcal, however, has to be done with some care when, as in our case, the number of telescopes is small. As a starting point it was found useful to apply just a constant (in time) amplitude correction factor for each antenna during the whole observation. Here we note a difference between MERLIN and EVN data. In the case of MERLIN observations, the application of just a constant gain correction factor had only a minute impact on the resulting maps, (this was true both for the originally calibrated as well as the recalibrated data), whereas for most EVN maps the difference was readily noticeable. We attribute this to superior initial MERLIN calibration. Gradually decreasing the timeconstant for the gain correction variations, we found (by inspection of the maps, the fits to the data, the rms noise in the maps, and the applied gain corrections) that the MERLIN maps constantly improved as the timeconstant was decreased. This indicates that the main source of error in the MERLIN data has a short timeconstant, which is indicative of tropospheric origin, or possibly tracking errors due to e.g. wind. For the EVN data the situation is more complicated. Most maps improved when the timeconstant was made smaller, at least to a certain limit (which was not the same for all maps), while in two cases it was found to be detrimental to use amplitude selfcal at all. Thus, each EVN data set was treated individually with respect to selfcal, details are given in Table 3.

Normally, the CLEAN beam was taken to be an elliptical gaussian fit to the central portion of the synthesized dirty beam. In some cases, a smaller beam was used as well, in an attempt to bring out more information from the data. This is normally referred to as "superresolution". Although superresolution rests on an insecure theoretical foundation one should keep in mind that the use of a CLEAN beam to suppress the higher spatial frequencies is ad hoc in the first place (it is the Fourier transform of the *unconvolved* CLEAN components that fit the data), and that the structures of our sources are particularly simple. The danger with superresolution is that with a barely resolved source, there can be more than one set of CLEAN components that fit the data and produce identical maps when convolved with the "standard" ("full") beam. When convolved with a smaller beam, these differences may show up. We only use this technique in order to better estimate position angles and spectral indices, not to establish accurate source structures.

The similar mapping procedures used for both the MERLIN and EVN maps makes it interesting to compare the quality that we could attain. Let us adopt $\sigma/n^{1/2}$ (Wilkinson, 1983), where σ is the average noise per visibility and n the total number of visibilities, as a rough estimate of the expected theoretical limit for the rms noise per independent beam area in a map. (A more thorough estimate of the noise per beam area would require us to take into account the actual visibility noise and weighting applied to individual visibilities.) If we allow for the fact that by using the (noisy) data itself to derive telescope errors (selfcal) we feed back more noise into the map thereby raising the theoretically attainable "thermal" noise level (Cornwell, 1981), we find that with the MERLIN data maps were derived with rms noise, in regions containing no emission, close to the calculated theoretical noise limit, whereas in the case of EVN maps the actual achieved noise level is up to a factor of eight worse (see Table 3). Even without amplitude selfcal,

Table 3. Observational results

Source name	Redshift/ lin. scale[a] (pc/mas)	Array /band	Source flux[b] (Jy)	Peak map flux (Jy/beam)	Cleaned flux (Jy)	Synth. beam[c] (mas, deg)	Selfcal mode[d]/ time const.	Map rms noise[e], σ (mJy/beam)	σ/σ_{qth}[f]	Dynamic range[g]
NRAO140	1.258	EVN/*L*	3.1	2.2	3.2	14×10, 24	$a+p/2$	$\sim$ 2	$\sim$2	$\sim$ 220
	$5.4\,h^{-1}$	EVN/*C*	2.5	1.9	2.4	9×8, -43	$a+p/2$	$\sim$ 2	$\sim$1	$\sim$ 190
		MERLIN	–	2.4	2.4	81×64, 89	$a+p/0.1$	$\sim$ 0.6	$\sim$1	$\sim$ 900
3C120	0.033	EVN/*L*	4.3	2.3	2.6	38×30, $-$ 7	$a+p/3$	$\sim$ 3	$\sim$3	$\sim$ 150
	$0.5\,h^{-1}$	EVN/*C*	2.7	1.7	1.9	11×10, -64	p	$\sim$ 4	$\sim$2	$\sim$ 85
		MERLIN	–	3.3	3.5	102×80, 89	$a+p/0.05$	$\sim$ 0.6	$\sim$1	$\sim$1200
3C179	0.846	EVN/*L*	2.1	0.3	0.3	25×24, -39	$a+p/99$	$\sim$ 1	$\sim$1	$\sim$ 70
	$4.9\,h^{-1}$	EVN/*C*	0.9	0.3	0.3	10×9, 85	p	$\sim$ 0.7	$\sim$1	$\sim$ 85
		MERLIN	–	0.3	0.3	80×80, 0	$a+p/0$[h]	$\sim$ 1	$\sim$1.5	$\sim$ 60
3C279	0.538	EVN/*L*	9.9	6.2	6.8	22×9, 16	$a+p/0.2$	$\sim$ 4	$\sim$2	$\sim$ 310
	$4.1\,h^{-1}$	EVN/*C*	13.4	6.9	6.9	14×9, -15	$a+p/2$	$\sim$ 9	$\sim$4	$\sim$ 150
		MERLIN[i]	–	10.6	10.6	98×95, 53	$a+p/0.01$	$\sim$ 1.2	$\sim$1.5	$\sim$1800
3C345	0.595	EVN/*L*	8.0	5.8	6.9	14×9, 21	$a+p/99$	$\sim$ 7	$\sim$8	$\sim$ 160
	$4.3\,h^{-1}$	EVN/*C*	11.9	8.0	8.4	10×9, -56	$a+p/2$	$\sim$13	$\sim$4	$\sim$ 120
		MERLIN	–	10.1	9.8	79×70, 88	$a+p/0.1$	$\sim$ 1.2	$\sim$2	$\sim$1800

Notes

[a] Using $H_0 = 100\,h$ km s^{-1} Mpc^{-1}, $q_0 = 0.1$, for the Hubble constant and the deceleration parameter respectively, and assuming a standard Friedmann cosmology

[b] As measured by Effelsberg during the VLBI observations

[c] Synthesized beam = CLEAN beam

[d] Mode of selfcalibration; p: phases only corrected, $a+p/t$: both amplitude and phases corrected, timeconstant t hours for the variation of the amplitude corrections

[e] As measured in several regions of the map where there is no detectable emission, given value is average. For the low-declination sources, 3C120 and 3C279, the side-lobe patterns cause the noise to be substantially higher due north and south of the cores

[f] Actual rms noise per beam in the map σ, divided by the calculated (as described in the text) quasi-thermal value σ_{qth}

[g] Defined as (peak flux in map)/5σ, where σ is the rms noise in the map. This is approximately equivalent to (peak flux in map)/(lowest "believable contour")

[h] Map made using Jodrell Bank software, selfcalibration performed integration by integration, no smoothing

[i] Figures refer to AIPS map. The OLAF map has $\sigma \sim 0.8$ mJy/beam, giving $\sigma/\sigma_{qth} \sim 1$, and a dynamic range of $\sim$2600

we could make MERLIN maps with rms noise within a factor of two of the theoretical limit, except in the case of 3C345 where the observations were affected by bad weather. (Here the use of amplitude selfcal lowered the rms noise in the map by a factor of approximately four.) Taking the similar mapping schemes and the comparable (except for a scale factor) UV coverages into account, we feel that the difference in noise level between EVN and MERLIN maps must arise before the hybrid mapping stage in the data reduction chain. This implies that correlation, fringe fitting, and/or calibration are possible causes. Another possibility is contamination of visibilities by source structure too large to map. We suspect the higher quality of the MERLIN maps is due to superior calibration, especially with regard to corrections for systematic non-closing effects; in the EVN case no attempt has been made to correct for such effects. This is corroborated both by simulations where systematic errors have been introduced on purpose (Wilkinson, 1983) and by the fact that reanalysis of old MERLIN data has produced improved maps (Davies et al., 1985).

In addition, the 3C279 MERLIN data were mapped by T.W.B. Muxlow with the Jodrell Bank OLAF (Off-Line Analysis Format) MAP program, using the "difference mapping" approach (R.G. Noble, A. Bailey, and T.W.B. Muxlow, unpublished). This procedure is also an interactive hybrid mapping method involving an iterative selfcalibration, fourier inversion/deconvolution loop, but furthermore, corrections can be made for non-closing errors in both amplitude and phase, i.e. baseline-dependent errors in the data can also be corrected for. Even with the new improved initial MERLIN calibration, when selfcal has been used to good advantage, residual baseline-dependent errors will at some stage be the limiting factor in the map quality. The applied corrections for non-closing errors were not greater than one percent in amplitude and 0°.2 in phase, but nevertheless the rather conspicuous north-south sidelobe pattern could be markedly reduced in this case of a strong low declination source.

3. Results

Our expectations of relatively simple source structures were borne out by the maps actually produced. Except in the case of 3C179, which is nearly unresolved, the maps are shown in Figs. 1–4. Data pertinent to the mapping results for all of our observations are listed in Table 3.

We now briefly review the radio structure on the arcsecond and mas scales, as well as the observational results of the present project for each source separately.

As a preliminary to these discussions it is useful to relate the angular sizes in the maps to actual physical (projected) linear dimensions in the respective sources. Using the values $H_0 = 100\,h\,\mathrm{km\,s^{-1}\,Mpc^{-1}}$ for the Hubble constant and $q_0 = 0.1$ for the deceleration parameter, we find that for 3C120 1 mas corresponds to approximately $0.5\,h^{-1}$ pc (or 1 kpc to $2h''$), whereas for the others we have that 1 mas roughly corresponds to $5\,h^{-1}$ pc (1 kpc to 200 h mas), i.e. the difference in linear scale is an order of magnitude (see also Table 3). We will note that observationally 3C120 stands out among the sources in the sample, and its relative proximity is clearly an important factor in this context.

NRAO 140

This quasar is unique among these superluminals in the sense that its relativistic bulk motion was postulated in order to resolve a discrepancy between the observed X-ray flux and that predicted by the inverse Compton process (Marscher and Broderick, 1981) before any structural changes had actually been observed to take place. Multifrequency mapping (Marscher and Broderick, 1985) now shows this source to have an extremely compact core, designated A_1, and an ~ 8 mas knotty jet, with components designated A_2, B, C, and D, extended along position angle (p.a.) $\sim 130°$. In addition the B component in the jet has a proper motion of 0.15 ± 0.01 mas yr^{-1}. The Compton problem requires relativistic bulk motion consistent with that derived from the observed proper motion. This structure accounts for almost all of the flux in the source; a weak component ~ 15 mas away along p.a. $\sim 145°$ and possibly an even weaker one further out completes the small scale picture. On the arcsecond scale observations with the WSRT, MERLIN, and VLA (Schilizzi and de Bruyn, 1983; Browne et al., 1982; Perley, 1982) all show a faint extended component $\sim 7''$ away from an unresolved core along p.a. $\sim 149°$; the WSRT map also shows an even fainter component $\sim 4''$ from the core on the opposite side, which cannot be seen in a very high dynamic range VLA map (Browne, 1986).

Maps produced from EVN observations of this, the most distant source in the sample are shown in Fig. 1a and b. On the 5 GHz map only the core can be seen as an elongated structure along p.a. $\sim 135°$, without trace of further, more extended emission. The 1.66 GHz map shows a simple, basically unresolved, component. However, inspection of the visibility data reveals that the source is not completely unresolved at L band and is, in fact, clearly resolved on all baselines involving Crimea, the ratio of the maximum to the minimum correlated amplitude on these baselines being greater than two. This fact seems to have been masked by the mapping process. Therefore, in an attempt to get the most out of our data, we used superresolution and model fitting. The results from both techniques indicate that a single elongated structure is a good model of the source; such a model fits the data better than any two-component model we have been able to devise. We also made superresolved 5 GHz maps. Here the elongation becomes more pronounced as the size of the convolving beam is decreased, and a more core-jet like structure emerges. The position angles of the structures at 1.66 and 5 GHz share the common value of $135° \pm 2°$.

Note that the resolution is comparable at the two frequencies; this is due to the participation of the Crimean telescope in the lower frequency observations. The differences between the maps are therefore probably related to spectral index effects. These are hard to quantify, however, because of insufficient resolution. From the superresolved maps, we estimate the jet spectral index $\alpha_{\nu(\mathrm{GHz}),\,\nu(\mathrm{GHz})}$ ($I_\nu \propto \nu^\alpha$) to be very approximately $\alpha_{5,\,1.66} = -0.5$ at an angular distance of ~ 8 mas from the core, corresponding to the location of components C and D. N.b. all spectral index calculation figures must be treated with caution because, in addition to possible inaccuracies in the map registrations, the absolute flux calibrations are not entirely reliable between different observing sessions, arrays, and frequencies. In neither case do we detect emission further out from the core, and furthermore, the MERLIN observations reveal nothing but an unresolved core, down to the thermal noise level (see Fig. 1c).

3C120

3C120 is the only (Seyfert) galaxy in the sample. It is also one of the brightest and most variable extragalactic radio sources, and is relatively nearby. The radio mas structure (Walker et al., 1982, 1984; Walker, 1985) has core-jet morphology, consisting of

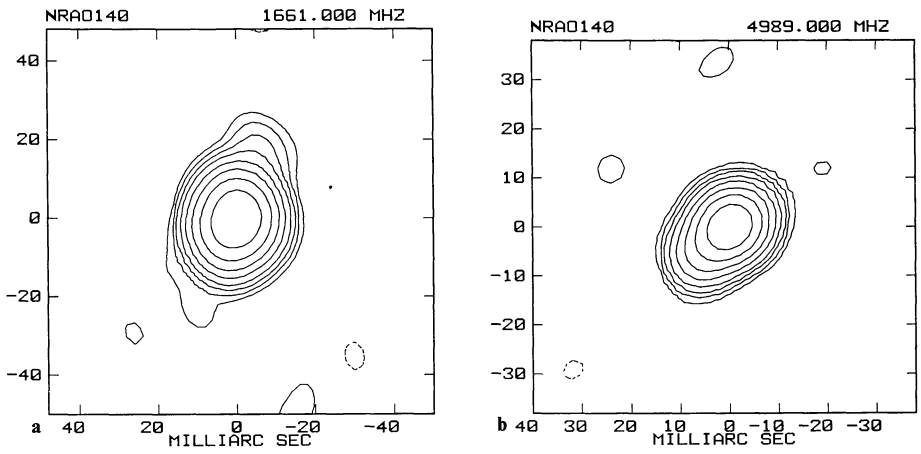

Fig. 1a and b. EVN maps of NRAO140 at 1.66 and 5 GHz. The contours are -0.5, 0.5, 1.0, 1.8, 3.2, 6.4, 12.5, 25, and 50% of the peak fluxes 2.2 and 1.9 Jy/beam. The 5σ levels corresponds to $\sim 0.5\%$ in both cases. All EVN maps have identical contour levels from the 3.2% level and upwards, the lowest level has always a negative contour as well, and the beams are well represented by the top contour

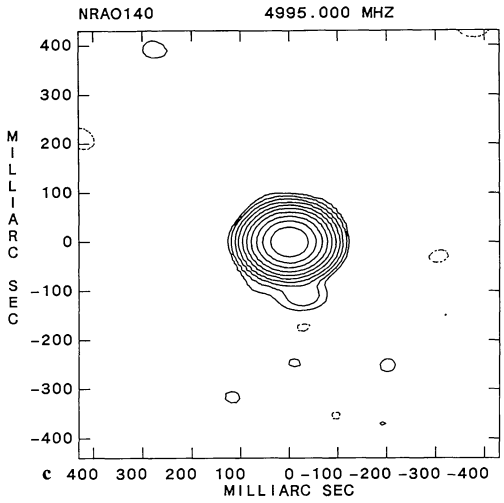

Fig. 1c. MERLIN map of NRAO140. Contours are -0.08, 0.08, 0.16, 0.35, 0.7, 1.5, 3.0, 6.0, 12.5, 25, and 50% of the peak flux of 2.4 Jy/beam. The 5σ level corresponds to $\sim 0.11\%$

several rapidly varying features extending along p.a. $\sim -100°$ away from the core. In the period 1980–84, four components were identified and measured to move roughly 2.5 mas yr^{-1}. Lower resolution 1.66 GHz VLBI observations (Benson et al., 1984; Walker, 1985) track the jet some 200 mas out from the core. It extends ~ 150 mas along p.a. $\sim -96°$, and then possibly curves southwards. Various VLA observations are also presented by these authors. In an *A* array map at 2 cm we can follow the jet $\sim 0\farcs6$ out from the core in p.a. $\sim -99°$, the brightness decreasing rather smoothly as the core distance increases, and there is weak emission $\sim 3\farcs8$ from the core at p.a. $\sim -100°$. This feature appears as a very distinct knot in the 6 cm *A* and *B* array maps, as well as in the 408 and 1666 MHz MERLIN maps (Browne et al., 1982). In these VLA maps we can follow the jet $\sim 15''$ as it gradually curves towards the northwest (NW), and in addition there is a knot $\sim 12''$ further out. This knot is at the end of the bright part of the jet in the 6 cm *C* array map; in the 18 cm *C* array and 6 cm *D* array maps there are extended lobes on both sides of the core, NW and SE, the SE lobe being the stronger of the two, i.e. the one on the opposite side from the mas and arcsecond jet.

Our EVN maps are shown in Fig. 2a and b. In the 1.66 GHz map we can follow a low brightness jet extending ~ 200 mas (~ 6 beamwidths) away from the core. The jet is not resolved perpendicular to its direction of extension. (Note that since this map has been made from observations using four telescopes only, the resolution is a factor of three lower than in e.g. the corresponding NRAO140 map.) The first ~ 150 mas of the jet are aligned along p.a. $\sim -98°$; further out the jet is possibly deflected southwards. The apparent core in the map is clearly extended and may be interpreted as a blend of the physical core and those jet knots which are within the beam. Going up by a factor of three in frequency and resolution, the 5 GHz map shows a compact core elongated in the general jet direction, but no significant extended or jet-like emission. In contrast the MERLIN map at the same frequency shows a smoothly fading jet in p.a. $\sim -100°$ which can be traced out to ~ 500 mas (~ 6 beamwidths) from the core; see Fig. 2c.

The MERLIN jet resembles that seen in the 2 cm VLA A array map. An estimate of the jet spectral index $\alpha_{15,5}$ gives values, both at ~ 200 mas and ~ 400–500 mas from the core, consistent with the value –0.7 proposed by Walker (1985) for most of the larger scale structure. Unfortunately our EVN observations only place an upper limit for $\alpha_{5,1.66}$ at ~ 50–100 mas from the core, $\alpha_{5,1.66} \lesssim 0$.

3C 179

3C179 is special in at least two, not necessarily unrelated, ways among these superluminals. It is the only one with a classical double lobe structure on the arcsecond scale. Also its core is an order of magnitude weaker than that of the others in the group. On the smallest (mas) scale, several epochs of observations using the largest available telescopes (Porcas, 1984), have demonstrated that a knot is receding from the core along p.a. $\sim -90°$, at roughly 0.19 mas yr^{-1}.

The present observations have very little to contribute to our picture of this source. Neither the EVN nor the MERLIN sensitivity is adequate to pick up possible extended structure on the angular scales to which they are sensitive, although the 5 GHz EVN observations marginally indicate that the core is extended in the E–W direction.

3C 279

Although structural variations, tentatively interpreted as relative motions between the two components in a double, were discovered in 1971 (Whitney et al.), 3C279 is the least studied of

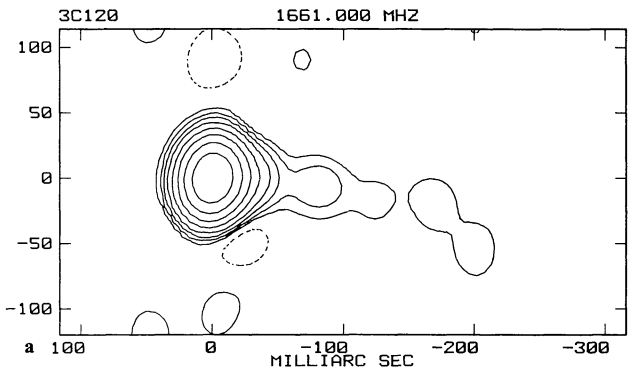

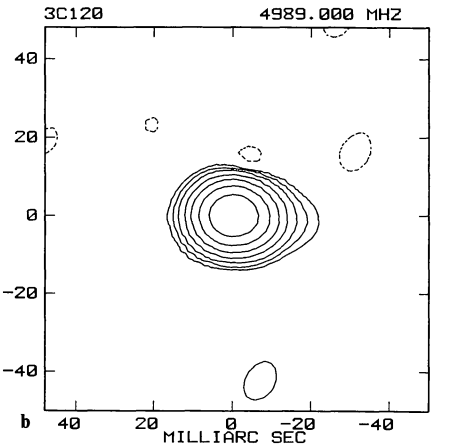

Fig. 2a and b. EVN maps of 3C120 at 1.66 and 5 GHz. At 1.66 GHz contours are 0.5, 1.0, 1.8, 3.2, ... and at 5 GHz the contours are 1.0, 1.8, 3.2, ... %. Peak fluxes are 2.3 and 1.7 Jy/beam, and the 5σ levels corresponds to ~0.7 and 1.2%, respectively

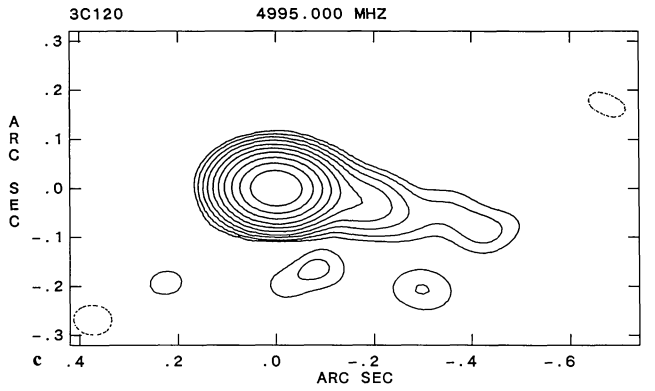

Fig. 2c. MERLIN map of 3C120, peak flux 3.3 Jy/beam and contours as in Fig. 1c. The 5σ level corresponds to ~0.08%

these superluminals. The arcsecond structure (de Pater and Perley, 1983) is that of a core and a one-sided jet extending 4".7 along p.a. ~206°. Five knots, labeled C to G, are identified in the jet. Their core distances increase from 0".095 and 0".58 for C and D respectively, to 4".7 for G, with spectral indices steepening from −0.75 for the inner knots to −0.92 and −1.11 for F and G respectively. The p.a. is 215° for C and within ±2° of the mean p.a. of 206° for the others. An anomalous diffuse steep-spectrum component ~11" away from the core along p.a. ~ −35° is also present in the MERLIN 408 MHz map (Browne et al., 1982). On the mas scale the structure is reported (Unwin and Biretta, 1984) to be a close double, separation ~1.2 mas along p.a. ~225° increasing at 0.17 mas yr^{-1}. The NE component has the flatter spectrum and is thus presumably the core which is consistent with the arcsecond appearance.

The strength and redshift of 3C279 are very similar to those of 3C345, however, the EVN maps resulting from the present observations bear little resemblance to each other, possibly indicating a significant difference in either or both of intrinsic structure and relative orientation. While 3C345 is clearly resolved at both frequencies, the opposite is true for 3C279; its core seems to be very compact indeed. If strong enough, the aforementioned C component should show up in our EVN maps, Fig. 3a and b. There is emission with a peak intensity at approximately the 15σ level in the 1.66 GHz map, located ~90 mas from the core at a p.a. of ~208°. This may be the C component, but it could possibly be part of the north-south sidelobe structure present in all our 3C279 (and 3C120) observations. On the basis of this observation alone it is not clear which interpretation is correct. There is nothing similar in the 5 GHz map. The apparent compactness of the core in 3C279 has prompted us to perform higher angular resolution observations (Pilbratt et al., 1987). The compactness is confirmed.

In the MERLIN observations the previously mentioned D component in 3C279 is detected, although in the AIPS map (Fig. 3c) the situation is somewhat confusing because of the proximity of the north-south sidelobe structure. In the map made using the OLAF software (Fig. 3d), however, not only is the D component clearly seen, but we can follow the jet ~4".7 out from the core along p.a. ~203°. Since the VLA at 15 GHz and MERLIN at 5 GHz have comparable beamsizes, we calculate the spectral index for the D component to be $\alpha_{15.5} = -0.7 \pm 0.1$. The peak surface brightness in the much weaker extended jet emission in the OLAF map agrees to within 20% of that in the VLA 6 cm map.

3C345

Associated with a 16th magnitude quasar, being strong and at high declination, 3C345 is not only the best studied of the superluminals but also a good representative of the group in the sense that it exhibits many of their common properties. From a compact core, which is self-absorbed at frequencies up to at least 10 GHz, a one-sided curved jet is defined by four steep-spectrum components, designated C4, C3, C2, and C1. The first three components were approximately 0.3, 2, and 4.5 mas distant from the core roughly at p.a. −130°, −83°, and −75° respectively in 1981 (Biretta et al., 1983; Unwin et al., 1983) and the fourth and most distant (C1) was very approximately 18 mas away from the core at a p.a. in the interval −67°±10° (Cohen et al., 1983b). Except for C1 these components all show proper motions with respect to the core which is stationary with respect to the nearby quasar NRAO512 (Bartel et al., 1984, 1986). The motion of C4 is unusual; in addition to following a non-radial path (Biretta et al., 1983) it also seems to be accelerating (Moore et al., 1983). The arcsecond jet seems to be a continuation of the mas jet; it reaches ~3" and the p.a. varies from −38° near the core to −32° at a hotspot at its end (Browne et al., 1982). In addition there is halo-like emission on a scale of 15" × 20" around the source (Schilizzi and de Bruyn, 1983).

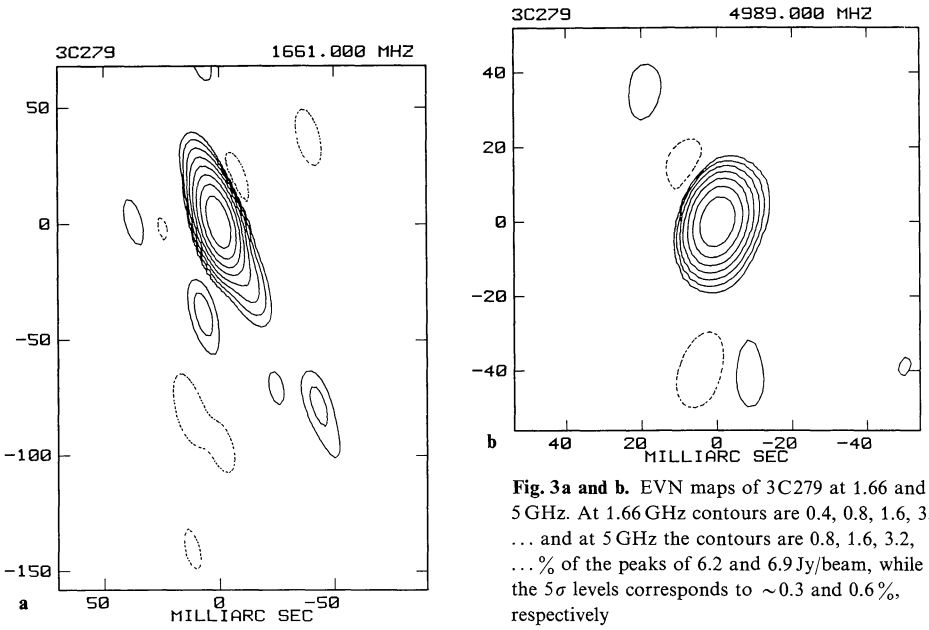

Fig. 3a and b. EVN maps of 3C279 at 1.66 and 5 GHz. At 1.66 GHz contours are 0.4, 0.8, 1.6, 3.2, ... and at 5 GHz the contours are 0.8, 1.6, 3.2, ... % of the peaks of 6.2 and 6.9 Jy/beam, while the 5σ levels corresponds to ~0.3 and 0.6 %, respectively

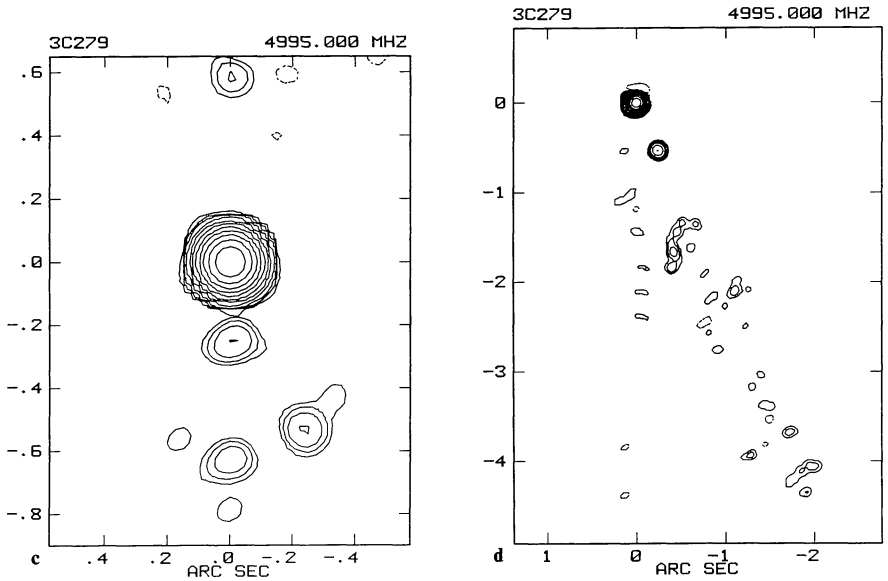

Fig. 3c and d. AIPS and OLAF MERLIN maps of 3C279. Contours are −0.07, 0.07, 0.12, 0.2, 0.4, 0.8, 1.6, 3.2, 6.4, 12.5, 25, and 50 % of the peak of 10.6 Jy/beam for the AIPS map. The OLAF map has a lowest contour of 0.04 %, otherwise the same, the peak is 10.2 Jy/beam. The 5σ levels are ~0.06 and 0.04 %, respectively. However, the main improvement in the OLAF map is the reduction in the north-south sidelobe levels which is the result of correcting for non-closing errors in the visibility data

Both EVN maps, Fig. 4a and b, show elongated structures, especially that at 1.66 GHz. Here we may, with some justification, talk about a jet emanating from the core and reaching out ~35 mas (~3 beamwidths) along p.a. ~ −49°. A closer inspection reveals that the ridge of maximum emission in the jet does not have a constant p.a. as the distance from the intensity peak increases. This peak is not the real core but is a blend of the core and the nearest components caused by our relatively low resolution. The 5 GHz map, on the other hand, only shows an elongated structure and here the intensity peak is probably the core. In order to estimate the p.a. as a function of the distance from the core along the jet we used superresolution. The results indicate that out to a distance of ~10 mas from the core, the p.a. is −66° ± 5°; this value is based on measurements in both maps and no difference between the two is discernible. Further out, in the range ~15 to ~30 mas from the core the 1.66 GHz map shows emission with p.a. −50° ± 3°. There is no emission on this scale in the 5 GHz map.

It is not possible to tell from our data alone whether this change of p.a. as a function of core distance is truly gradual or whether it is attributable to the individual components moving at different but constant position angles. In the rectilinear motion model (Cohen et al., 1983a) each section of the jet defines the orientation of the nozzle at an earlier epoch. In this regard it would be interesting to follow individual components over extended periods of time and radial distance, as they move out from the core. Clearly, low frequency (L and/or S band) global VLBI observations are important here. The rectilinear motion model may already be in trouble, however, because of the peculiar non-radial motion of the C4 component already mentioned. It would

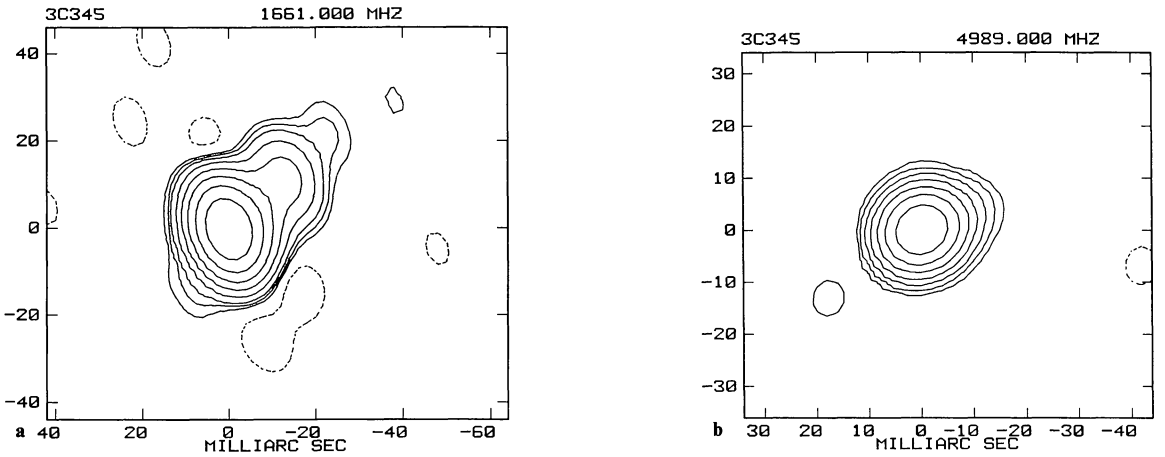

Figs. 4a and b. EVN maps of 3C 345 at 1.66 and 5 GHz. Contours are 0.6, 1.0, 1.6, 3.2, ... and 0.8, 1.6, 3.2 ... % of the peak fluxes of 5.8 and 8.0 Jy/beam at 1.66 and 5 GHz. The 5σ levels corresponds to ~ 0.6 and 0.8 %, respectively

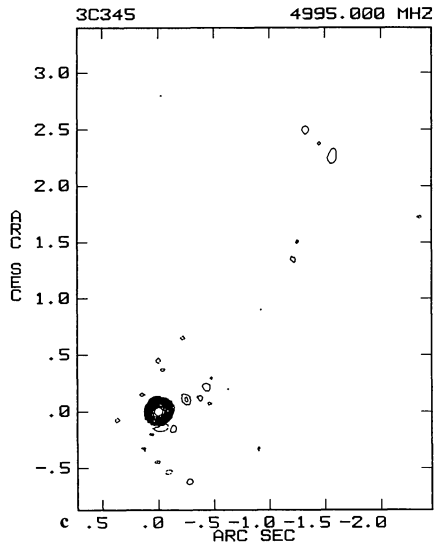

Fig. 4c. MERLIN map of 3C345, contours are -0.05, 0.05, 0.1, 0.2, 0.4, 0.8, 1.6, 3.2, 6.4, 12.5, 25, and 50 % of the peak flux of 10.1 Jy/beam. The 5σ level corresponds to ~ 0.06 %

also be extremely interesting to be able to follow the jet further out than has hitherto been possible. Unfortunately, our MERLIN observations (Fig. 4c) give no help in this respect.

However, while not showing a continuous jet, the MERLIN map does display weak jet emission $\sim 1''.9$ and $2''.8$ away from the core. The latter can most probably be identified with a relatively much stronger feature in the 1.66 GHz MERLIN map (Browne et al., 1982). The spectral index calculation is complicated by the question of to what degree the feature is resolved, but it is likely that $\alpha_{5,1.66}$ is steeper than ~ -1.0 for this feature, while the corresponding upper limit for the jet emission on the whole is -0.5.

As was the case for NRAO 140, the resolution is very similar at the two EVN frequencies; thus the differences between the corresponding maps are related to spectral index effects, and again, these are hard to quantify with the present resolution. From the superresolved maps we estimate $\alpha_{5,1.66}$ roughly as ~ -0.5, in the range 10–20 mas from the core.

4. Discussion

The main objective of this work was to investigate the structure of the superluminal sources on scales of tens to several hundreds of mas i.e. between the previously published VLBI data and the lower frequency MERLIN data. In particular we sought to investigate the nature of the beam, and the blobs observed on the mas scale, as the core distance increases. Hence our choices of relatively low observing frequencies and short baselines. The observational results are easy to summarize: given the present instrumental limitations of UV coverage and dynamic range, save for 3C120 we are on the whole unable to follow the jets within our primary range of interest (although blobs of emission are detected much further out for 3C279 and 3C345). Thus, *if the fundamental properties of the beam model are correct, then this is despite the fact that the beams are actually there.* What then, renders a beam visible or invisible?

We believe, as has now been demonstrated in the case of Cygnus A (Perley et al., 1984), that at some level a continuous beam will show up as a visible jet along its full extent. The question of visibility is thus governed by the strength of the jet emission in relation to the instrumental parameters. The most obvious instrumental limitations to our detection of further extended emission are insufficient UV coverage and/or sensitivity. It is thus important to take these into account before any discussion of the source physics resulting from our observations can take place.

The most obvious limitation of the UV coverage is the truncation given by the longest baseline, putting an upper limit to the resolution that can be obtained. In addition the maximum size of the unsampled regions ("holes") in the UV plane coverage will impose an upper limit on the size of a region with *arbitrary* intensity distribution that can be mapped, the shortest baseline will determine the maximum angular extent of any source structure to which the interferometer is sensitive, while the bandwidth ("delay beam") and the visibility averaging time will restrict the size of the region within which isolated compact features can be mapped. For the present observations the relevant limit to the field of view is presumably neither determined by the holes in the UV coverage nor by the shortest spacing, but because of the simple core-jet structure of these sources the isolated source case is rather more appropriate.

Using the estimates of Thompson (1982) we conclude that the bandwidth is not an important factor as long as the mapsize is no

larger than many hundred beamwidths in the MERLIN case, and even more negligible in the case of EVN maps; whereas the visibility averaging times used allow mapsizes of the order of a hundred beamwidths. Furthermore, from MERLIN experience Wilkinson (1983) argues that with a four- (six-) station quasi-random array (like MERLIN or EVN) it should be possible to map a rectangular box of arbitrary brightness distribution of dimension up to 10 (20) beamwidths (on a side) and a linear (core-jet) structure out to a maximum of 20 (50) beamwidths from the core. In the latter case the apparent improvement is due to the fact that most of the map is blank, making the number of pixels showing emission still smaller than in the former case. This criterion applied to our EVN observations yields upper limits to the size of any linear structure that can be mapped of ~ 500 mas and ~ 150 mas at 1.66 GHz and 5 GHz respectively, and correspondingly for the MERLIN observations in the range 3″ to 4″. We conclude that *the absence of further extended emission in our maps is not simply related to insufficient UV coverage.*

Instead, it seems that we must accept that, on the angular scales of primary interest in our present observations, the brightness of the jet emission simply fades below observable levels quickly with increasing distance from the core. Thus, in order to trace these jets even only a limited number of beamwidths outwards, maps reliably showing even weaker emission are required; i.e. we would need maps with higher dynamic range, or more sensitive observations, preferably both. However, in terms of dynamic range, our present EVN maps are of comparable quality to the very high (mas) resolution maps that show the features exhibiting proper motions, and our MERLIN maps are an order of magnitude better. Bearing in mind that it is always a difficult task to compare maps made using different arrays, it seems fair to claim that *these sources do display a brighter and more blobby radio emission on the mas scale*, and occasional local higher brightness features in the arcsecond angular resolution observations, such as are seen in the MERLIN data, that are absent on the intermediate angular scales. Consequently it appears that the mechanisms, whether intrinsic or extrinsic to the beam itself, operating at the parsec and kpc scales respectively and giving rise to the blobs of locally stronger radio emission in those regions are not at work here.

The parsec scale blobs must form very close to the core; in the cases of 3C120 and 3C345 moving knots have been detected within 1 mas (Walker, 1985) and 0.4 mas (Moore et al., 1983) respectively, corresponding to $\sim 0.5\,h^{-1}$ pc and $\sim 3\,h^{-1}$ pc, projected distances. Furthermore, these numbers are of course only upper limits given by the maximum resolution obtainable in present-day VLBI observations. The observations indicate that the formation of the blobs is taking place just outside the region around the central powerhouse identified as the broad emission-line region (BLR) in quasars and active galactic nuclei (e.g. Mathews and Capriotti, 1985). These distinct bright features are presumably created where the underlying bulk flow in the beam becomes dissipative, i.e. where some bulk kinetic energy is converted to random relativistic electron motion. A straightforward method of introducing dissipation into the flow is by means of shock fronts. Whether the shocks themselves are excited by instabilities or collisions, the BLR region constitutes a plausible environment for their formation. Natural obstacles causing collisions are the BLR clouds or the even larger structures that may be involved in the formation of these clouds (Perry and Dyson, 1985). Also, at this distance from the central powerhouse collimation of the beam must have taken place (or take place), and it is not an unreasonables idea to envisage shocks being caused by this process. Either way, the conditions here are special in the sense that they are not reproduced further out along the beam. The blobs, however they are formed, display proper motions, and are observed to decay in brightness with time constants of a few years, possibly due to adiabatic expansion (Unwin et al., 1983). Even for the relatively well-studied sources 3C273 and 3C345, the available observations are consistent with a wide range of fading laws. For 3C273 the data are consistent with a power-law decay of the form $S/S_0 = (t - t_0)^{\eta}$, where t is epoch (Unwin et al., 1985). Depending on the decay mechanism, η will have different values. The preferred choice in this case seems to be $\eta = 2\alpha - 1$, corresponding to adiabatic expansion with continuous re-acceleration with energy index $2\alpha - 1$. Using this model as an illustrative example, and assuming $\alpha = -0.7$ for a typical blob, in a ten year period we get $S/S_0 = 10^{-2.4}$. Consequently, since the typical proper motions are of the order of only a few tenths of a mas (except 3C120 ~ 2.5 mas) per year (e.g. Cohen and Unwin, 1984), these blobs will have decayed and become unobservably weak well before reaching the distances from the cores corresponding to our present EVN observations. Note that the magnetic field has to be considerably stronger than 1 milligauss for electron ageing due to synchrotron losses to be important in this respect.

In this context it is worth remarking that it is not inconceivable that the velocities corresponding to observed proper motions (the superluminal motions) of high brightness features may differ from the velocity of the bulk flow in a beam. Here velocity differences for blobs in the same object may reflect natural consequences of dissimilar "birth and/or life" conditions rather than (or in addition to) variations in the bulk flow.

We interpret the rapid fading of the jets as an indication that, after having traversed the initial more turbulent parsecscale region where the processes of collimation and formation of blobs take place, the flow is more laminar, and that the efficiency of the mechanism creating the moving radio emitting features is high only in a restricted region. Outside this region we envisage the beam to propagate with relatively small losses due to friction (viscous dissipation) with the surrounding medium. In a (very) simplistic model of the visible jet, we may think of it as being made up of a train of fading blobs moving outwards at constant velocities. If no new blobs are created further out, the jet brightness I, at a given distance R from the core, will depend on the time taken for a blob to get there. The result is a beam where the intensity of the radio emission is decreasing rapidly as a function of R. Using the figures in our earlier example, we get $I \propto R^{\xi}$, where $\xi = -2.4$. In addition, we will have to take the locally produced radio emission into account, e.g. that produced by friction. It is clear that an observational determination of I as a function of R will require mapping of the *jet* emission itself with higher dynamic range than has hitherto been achieved. Regrettably, the data do not allow us to produce a value for ξ, not even in the case of 3C120.

Although too weak to be well mapped on subarcsecond scales in the present observations, these sources, with the exception of NRAO140, display extended jet emission strong enough on arcsecond scales to be mapped by MERLIN at lower frequencies (Browne et al., 1982). Using, for illustrative purposes only, a "normal" steep spectrum spectral index of $\alpha = -0.7$ for this larger scale jet emission, and assuming the jets to be unresolved in the perpendicular direction, we expect about one tenth of the flux per beam at 4995 MHz as compared to at 1666 MHz, which is consistent with our MERLIN observations.

We note in passing that the beam just described, having laminar flow and minor friction losses, is an efficient beam in terms of energy transport. This is an important observation in the

context of the problem of the origin of the observed onesidedness of the jets in these sources on arcsecond scales (reviewed by e.g. Bridle and Perley, 1984). Our observations thus demand that any scheme requiring these jets to slow down from relativistic to subrelativistic velocities between the mas and arcsecond scales should be constrained to do it without generating excessive amounts of radio emission.

Acknowledgements. We are grateful to Dr. T.W.B. Muxlow for taking care of the tedious task of calibrating (and recalibrating) the MERLIN data, and for running MAP on some of our data. We are also indebted to everybody involved in the operation of MERLIN at Jodrell Bank, and the EVN, including Crimea and Torun, at the participating observatories, as well as to Dr. D.A. Graham and W. Alef and to the MPIfR correlator staff for help during correlation.

Dr. I.W.A. Browne gave valuable comments and suggestions for improvements on an earlier version of this paper. We also wish to thank Drs. L.B. Bååth and P.J. Diamond for numerous helpful discussions about VLBI data reduction.

Onsala Space Observatory is operated by Chalmers University of Technology, Göteborg, with financial support from the Swedish Natural Science Research Council (NFR).

References

Baars, J.W.M., Genzel, R., Pauliny-Toth, I.I.K., Witzel, A.: 1977, *Astron. Astrophys.* **61**, 99

Bartel, N., Ratner, M.I., Shapiro, I.I., Herring, T.A., Corey, B.E.: 1984, in *VLBI and Compact Radio Sources*, *IAU Symp.* **110**, eds. R. Fanti et al., Reidel, Dordrecht, p. 113

Bartel, N., Herring, T.A., Ratner, M.I., Shapiro, I.I., Corey, B.E.: 1986, *Nature* **319**, 733

Benson, J.M., Walker, R.C., Seielstad, G.A., Unwin, S.C.: 1984, in *VLBI and Compact Radio Sources*, *IAU Symp.* **110**, eds. R. Fanti et al., Reidel, Dordrecht, p. 125

Biretta, J.A., Cohen, M.H., Unwin, S.C., Pauliny-Toth, I.I.K.: 1983, *Nature* **306**, 42

Blandford, R.D., Königl, A.: 1979, *Astrophys. J.* **232**, 34

Bridle, A.H., Perley, R.A.: 1984, *Ann. Rev. Astron. Astrophys.* **22**, 319

Browne, I.W.A., Clark, R.R., Moore, P.K., Muxlow, T.W.B., Wilkinson, P.N., Cohen, M.H., Porcas, R.W.: 1982, *Nature* **299**, 788

Browne, I.W.A.: 1986 (private communication)

Clark, B.G.: 1973, *Proc. IEEE* **61**, 1242

Cohen, M.H., Cannon, W., Purcell, G.H., Shaffer, D.B., Broderick, J.J., Kellermann, K.I., Jauncey, D.L.: 1971, *Astrophys. J.* **170**, 207

Cohen, M.H., Moffet, A.T., Romney, J.D., Schilizzi, R.T., Shaffer, D.B., Kellermann, K.I., Purcell, G.H., Grove, G., Swenson, Jr., G.W., Yen, J.L., Pauliny-Toth, I.I.K., Preuss, E., Witzel, A., Graham, D.: 1975, *Astrophys. J.* **201**, 249

Cohen, M.H., Unwin, S.C., Pearson, T.J., Seielstad, G.A., Simon, R.S., Linfield, R.P., Walker, R.C.: 1983a, *Astrophys. J. (Letters)* **269**, L1

Cohen, M.H., Unwin, S.C., Lind, K.R., Moffet, A.T., Simon, R.S., Wilkinson, P.N., Spencer, R.E., Booth, R.S., Nicolson, G.D., Niell, A.E., Young, L.E.: 1983b, *Astrophys. J.* **272**, 383

Cohen, M.H., Unwin, S.C.: 1984, in *VLBI and Compact Radio Sources*, *IAU Symp.* **110**, eds. R. Fanti et al., Reidel, Dordrecht, p. 95

Cornwell, T.: 1981, *VLA Scientific Memo 135*, NRAO

Davies, R.J., Muxlow, T.W.B., Conway, R.G.: 1985, *Nature* **318**, 343

Marscher, A.P., Broderick, J.J.: 1981, *Astrophys. J. (Letters)* **247**, L49

Marscher, A.P., Broderick, J.J.: 1985, *Astrophys. J.* **290**, 735

Mathews, W.G., Capriotti, E.R.: 1985, in *Astrophysics of Active Galaxies and Quasi-Stellar Objects*, ed. J.S. Miller, University Science Books and Oxford University Press, p. 185

Moore, R.L., Readhead, A.C.S., Bååth, L.: 1983, *Nature* **306**, 44

Muxlow, T.W.B.: 1986 (private communication)

de Pater, I., Perley, R.A.: 1983, *Astrophys. J.* **273**, 64

Pearson, T.J., Unwin, S.C., Cohen, M.H., Linfield, R.P., Readhead, A.C.S., Seielstad, G.A., Simon, R.S., Walker, R.C.: 1981, *Nature* **290**, 365

Pearson, T.J., Readhead, A.C.S.: 1984, *Ann. Rev. Astron. Astrophys.* **22**, 97

Perley, R.A.: 1982, *Astron. J.* **87**, 859

Perley, R.A., Dreher, J.W., Cowan, J.J.: 1984, *Astrophys. J. (Letters)* **285**, L35

Perry, J.J., Dyson, J.E.: 1985, *Monthly Notices Roy. Astron. Soc.* **213**, 665

Pilbratt, G., Booth, R.S., Porcas, R.W., Nicolson, G.D.: 1987 (in preparation)

Porcas, R.W.: 1984, in *VLBI and Compact Radio Sources*, *IAU Symp.* **110**, eds. R. Fanti et al., Reidel, Dordrecht, p. 157

Schilizzi, R.T., de Bruyn, A.G.: 1983, *Nature* **303**, 26

Thompson, A.R.: 1982, in *Synthesis Mapping*, Proc. of the NRAO-VLA Workshop, June 1982, eds. A.R. Thompson, L.R. D'Addario, Chap. 5

Unwin, S.C., Cohen, M.H., Pearson, T.J., Seielstad, G.A., Simon, R.S., Linfield, R.P., Walker, R.C.: 1983, *Astrophys. J.* **271**, 536

Unwin, S.C., Biretta, J.A.: 1984, in *VLBI and Compact Radio Sources*, *IAU Symp.* **110**, eds. R. Fanti et al., Reidel, Dordrecht, p. 105

Unwin, S.C., Cohen, M.H., Biretta, J.A., Pearson, T.J., Seielstad, G.A., Walker, R.C., Simon, R.S., Linfield, R.P.: 1985, *Astrophys. J.* **289**, 109

Walker, R.C., Seielstad, G.A., Simon, R.S., Unwin, S.C., Cohen, M.H., Pearson, T.J., Linfield, R.P.: 1982, *Astrophys. J.* **257**, 56

Walker, R.C., Benson, J.M., Seielstad, G.A., Unwin, S.C.: 1984, in *VLBI and Compact Radio Sources*, *IAU Symp.* **110**, eds. R. Fanti et al., Reidel, Dordrecht, p. 121

Walker, R.C.: 1985, in *Physics of Energy Transport in Extragalactic Radio Sources*, Proc. of NRAO Workshop No. 9, eds. A.H. Bridle, J.A. Eilek, p. 20

Whitney, A.R., Shapiro, I.I., Rogers, A.E.E., Robertson, D.S., Knight, C.A., Clark, T.A., Goldstein, R.M., Marandino, G.E., Vandenberg, N.R.: 1971, *Science* **173**, 225

Wilkinson, P.N.: 1983, in *Very Long Baseline Interferometry Techniques*, CNES Conference 1982, p. 375